Pressure-induced irreversible amorphization and metallization with a structural phase transition in arsenic telluride

Article *in* Journal of Materials Chemistry C · November 2017
DOI: 10.1039/C7TC03309E

CITATIONS
3

READS
20

8 authors, including:


Lidong Dai
Chinese Academy of Sciences
67 PUBLICATIONS **584** CITATIONS
SEE PROFILE


Yukai Zhuang
Chinese Academy of Sciences
10 PUBLICATIONS **25** CITATIONS
SEE PROFILE


Heping Li
Chinese Academy of Sciences
57 PUBLICATIONS **275** CITATIONS
SEE PROFILE


Lei Wu
Institute of Geochemistry, Chinese Academy of Sciences
16 PUBLICATIONS **59** CITATIONS
SEE PROFILE

Journal of
Materials Chemistry C

Accepted Manuscript

This article can be cited before page numbers have been issued, to do this please use: L. dai, Y. Zhuang, H. Li, L. Wu, H. Hu, K. Liu, L. Yang and C. Pu, *J. Mater. Chem. C*, 2017, DOI: 10.1039/C7TC03309E.

ROYAL SOCIETY OF CHEMISTRY

rsc.li/materials-c

View Article Online
DOI: 10.1039/C7TC03309E

Journal Name

ARTICLE

Received 00th January 20xx,
Accepted 00th January 20xx

DOI: 10.1039/x0xx00000x

www.rsc.org/

Pressure-induced irreversible amorphization and metallization with a structural phase transition in arsenic telluride

Lidong Dai[a*‡], Yukai Zhuang[ab‡], Heping Li[a], Lei Wu[a], Haiying Hu[a], Kaixiang Liu[ab], Linfei Yang[ab] and Chang Pu[ab]

The structural, vibrational and electronic properties of α-As_2Te_3 under different pressure environments were investigated using a diamond-anvil cell (DAC) in conjunction with AC impedance spectroscopy, Raman spectroscopy, atomic force microscopy and high-resolution transmission electron microscopy up to ~25 GPa. Under non-hydrostatic conditions, α-As_2Te_3 endured a structural phase transition at ~6 GPa, and a ~2 GPa delay in the transition point was observed under hydrostatic conditions. With increasing pressure, amorphization and metallization simultaneously appeared at ~11 GPa, as characterized by the Raman spectra and temperature-dependent conductivity results. We found that both amorphization and metallization were irreversible after decompression under non-hydrostatic conditions. However, under hydrostatic conditions, both amorphization and metallization were reversible. The unique properties displayed by α-As_2Te_3 under different pressure environments may be attributed to the effects of deviatoric stresses and the interlayer interaction constrained by the pressure medium.

Introduction

Since its discovery in ice (H_2O), pressure-induced amorphization (PIA) has been widely accepted as an important condensed matter phenomenon.[1-2] The thermodynamic and disorder basis for PIA greatly differs from the thermally induced rapid quenching.[1, 3] In some cases, PIA is a useful means to reveal new amorphous states for practical industrial applications, which has been observed in many materials, such as ice,[4] SiO_2,[5] and Zn_2GeO_4.[6] However, the underlying mechanism of PIA still remains a very controversial issue, among which "thermodynamic melting" [7] and "negative thermal expansion" (NTE) may possess possible connections with PIA.[8] Furthermore, a recent study showed that previously reported PIAs may be strongly correlated with the pressurization environments.[3] As a quasi-layered structural A_2B_3-type compound, α-As_2Te_3 is a monoclinic phase (space group $C2/m$) linked by weak van der Waals (vdW) interlayer forces, possessing an indirect band gap of 0.48 eV at ambient conditions.[9-12] Due to a relatively narrow band gap semi-conductor for α-As_2Te_3, it is possible to exhibit one unusual electronic behaviour at higher pressures. Pressure has served as a powerful tool to induce the metallization of many layered materials[13-14] and has given rise to many novel physical phenomena under various conditions.[13, 15] For example, MoS_2 was recently shown to undergo a pressure-induced permanent semiconductor-to-metal transition under non-hydrostatic compression, which may be attributed to deviatoric stresses and a reduction of the interlayer interaction.[15] Therefore, the pressurization environment may be a key factor for the final layered material after decompression. Thus far, reversible amorphization has been achieved in some main group compounds, such as SnI_4, $LiKSO_4$, $Ca(OH)_2$, clathrasils and berlinite $AlPO_4$, by annealing,[16-20] in which only the lattice participates in the intriguing structure transformation. The study of pressurization environments involved in PIA and permanent metallization could provide a more comprehensive understanding of layered structured materials under the function of deviatoric stresses.

In this work, we reported a structural phase transition, a crystalline-to-amorphous transformation and metallization, under both non-hydrostatic and hydrostatic conditions up to ~25 GPa using a diamond-anvil cell (DAC) in conjunction with impedance spectroscopy, Raman spectroscopy, atomic force microscopy (AFM) and high-resolution transmission electron microscopy (HRTEM). The selected-area electron diffraction patterns by HRTEM analysis are performed for the recovered crystalline phases after decompression in order to further disclose whether they are isostructural with the initial α-As_2Te_3 phase. In addition, the amorphization and metallization of the arsenic telluride were irreversible under non-hydrostatic conditions but reversible under hydrostatic conditions.

[a] Key Laboratory of High-Temperature and High-Pressure Study of the Earth's Interior, Institute of Geochemistry, Chinese Academy of Sciences, Guiyang, Guizhou 550081, China
[b] University of Chinese Academy of Sciences, Beijing 100049, China

*Correspondence to: L. Dai, E-mail: dailidong@vip.gyig.ac.cn
‡ These authors contributed equally to this work

View Article Online
DOI: 10.1039/C7TC03309E

Experimental

A commercially available 99.999% α-As_2Te_3 powder sample was purchased from Alfa-Aesar. The high-pressure electrical studies were performed using a DAC with an anvil culet size of 300 μm. T-301 stainless steel was used as the gasket and pre-indented to a thickness of 40 μm, then a 180 μm hole was drilled in the centre with a laser. The mixed powder of boron nitride and epoxy was then compressed into the hole, and another 100 μm hole was drilled into the centre as the insulating sample chamber. The pressure was calibrated with the displacement of the Cr^{3+} fluorescence peak of a ruby sphere.[21] The electrical conductivities of the sample were measured using a Solartron-1260 impedance spectroscopy analyser at frequencies of 10^{-1}–10^{7} Hz. Experimental methods and the measurement process have been previously described in detail.[22-23] The deformation of the diamond anvils was fully considered during the measurements.[24]

Raman spectra were acquired using a Renishaw 2000 Micro-Confocal Raman spectrometer (TCS SP8, Leica) equipped with an Olympus CCD camera. The spectra were collected in the quasi-backscattering geometry using an argon ion laser (Spectra Physics; 514.5 nm, power <1 mW) in the range of 300–550 cm^{-1} with a spectral resolution of 1.0 cm^{-1}. The mixture of methanol and ethanol at a 4:1 volume ratio was adopted as a pressure medium to provide hydrostatic conditions, and no pressure medium was used for non-hydrostatic conditions. The collection time for the Raman spectra was 600 seconds at each pressure point. To avoid pressure oscillation, the DAC pressure equilibration time was 1 h at each pressure point before the spectral acquisition. Raman spectra were fitted using the PeakFit software. A linear baseline calibration was applied with a fitting using the Lorenztian curve. All observations from the AFM and TEM images were obtained via a Multimode 8 mass spectrometer (Bruker) and Tecnai G2 F20 S-TWIN TMP, respectively.

Results and discussion

To study the high-pressure structural behaviour of α-As_2Te_3, Raman spectroscopy was performed under non-hydrostatic and hydrostatic conditions. The Raman spectra and corresponding experimental results during compression and decompression are shown in Fig. 1 and Table 1. In the present work, we observed the Raman-active modes in α-As_2Te_3 at peak positions of 120 cm^{-1} (A_g^4) and another two high-frequency modes between 170 and 200 cm^{-1} (A_g^9 and A_g^{10}), which are consistent with previously reported theoretical calculation results.[25]

From Fig. 1b and 1c, the changes of both the Raman shift and the full-width at half-maximum (FWHM) for the three modes with increasing pressure had two critical points (~6 and ~11 GPa) under non-hydrostatic conditions. At ~6 GPa, the A_g^9 and A_g^{10} modes disappeared, and the trend of the A_g^4 mode changed, which may be owed to a phase transition from the α phase to β phase.[9, 26] Generally, a pressure-induced phase transition is accompanied by a considerable change of the FWHM in certain materials.[27-28] Moreover, the A_g^4 mode also disappeared at ~11 GPa, indicating the occurrence of a crystalline-to-amorphous transformation (Fig. 1a). In fact, similar crystalline-to-amorphous transformations have been discovered in many solid-state materials.[5, 29-30] With increasing pressure, the degree of lattice distortion becomes more intense, and the original crystalline sample may be compressed far beyond the limit of its thermodynamic stability at some critical pressure point. Furthermore, enduring a non-equilibrium and kinetically hindered process may be possible, which will restrain the formation of the stable crystalline phase by kinetic effects.[31] In other words, the crystal structure of α-As_2Te_3 became unstable and transformed to an amorphous state above ~11 GPa.

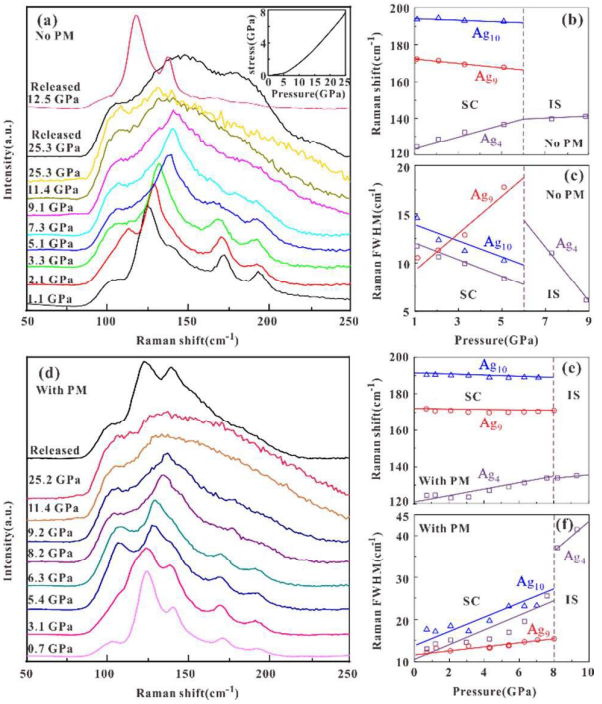

Fig. 1 Raman spectroscopic results of α-As_2Te_3 at high pressures. (a) and (d) Raman spectra at representative pressure points under non-hydrostatic and hydrostatic conditions, respectively. Inset: the positive correlation property between the deviatoric stress and pressure. (b) and (c) The Raman shift and FWHM of the selected modes with increasing pressure under non-hydrostatic conditions, respectively. The straight lines serve as visual guides. (e) and (f) The Raman shift and FWHM of the selected modes with increasing pressure under hydrostatic conditions, respectively. The straight lines serve as visual guides. PM: pressure medium.

In addition, as described in Fig. 1e and 1f, the Raman shift and FWHM results clearly show that the pressure-induced change point of the structural phase transition under hydrostatic conditions at ~8 GPa was delayed by ~2 GPa as compared to that under non-hydrostatic conditions, which is possibly related to a discrepancy in the pressure environments. Under non-hydrostatic conditions, a relatively strong deviatoric stress facilitates interlayer slide, resulting in the structural phase transition. Interestingly, the amorphous transformation point also occurred at ~11 GPa under hydrostatic conditions, which these are usually no longer hydrostatic above 10 GPa, although comparatively it will still be more hydrostatic than omission of a pressure transmitting medium.[32] Under hydrostatic conditions, the Raman modes of α-As_2Te_3 were reversible (Fig. 1d). However, under non-hydrostatic

View Article Online
DOI: 10.1039/C7TC03309E

conditions, these modes were reversible upon decompression from 12.5 GPa and irreversible upon decompression from 25.3 GPa (Fig. 1a). This phenomenon may be attributed to the following two aspects: (1) a sufficient pressure is crucial to break the thermodynamic stability of the lattice structure, which restrains the recovery of the stable crystalline phase and results in the formation of irreversible PIA; (2) deviatoric stress driven under non-hydrostatic conditions facilitates the transformation of the long-range order of the lattice to long-range correlated disorder (as shown in the inset of Fig. 1a, the deviatoric stresses reach ~2 and 8 GPa, while the centre pressures are 12 and 25 GPa, respectively). The irreversible amorphization has also occurred in another material under non-hydrostatic conditions due to irreversible lattice distortion.[33]

Table 1 Summary of experiments

	Phase transition	Amorphization	Decompression from ~16 GPa	Decompression from ~25 GPa
No PM	~6 GPa	~11 GPa	Reversible	Irreversible
With PM	~8 GPa	~11 GPa	–	Reversible

The representative Nyquist plots from impedance spectroscopy at different pressures are shown under non-hydrostatic conditions in Fig. 2 to understand the electrical properties of α-As_2Te_3. The semi-circular arc gradually decreased, and the grain interior resistance disappeared at approximately ~2 GPa. In addition, the impedance spectroscopy in the high-pressure region (>2 GPa) only displayed in the fourth quadrant (Fig. 2a, inset). This phenomenon indicates that the electronic crystal structure of α-As_2Te_3 greatly changed in this interval, demonstrating pressure-induced electronic polarization.[34]

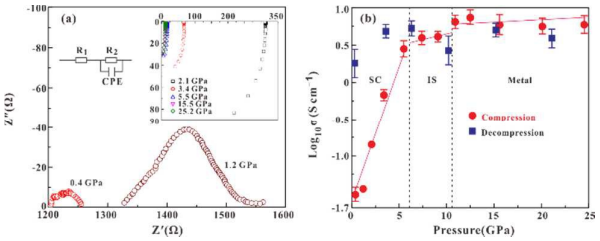

Fig. 2 (a) Nyquist plots from the impedance spectra of α-As_2Te_3 at different pressures. (b) Pressure-dependent electrical conductivity of α-As_2Te_3.

From Fig. 2b, the electrical conductivity abruptly increased up to a pressure of ~6 GPa and gradually increased between 6~11 GPa under non-hydrostatic conditions. We attribute the inflection point to the phase transition, which coincides with the Raman data. We also observed a step point at ~11 GPa. When the pressure is higher than ~11 GPa, the conductivity was stable. The pressure derivative of the electrical conductivity changes displayed a changed value at this point, confirming that the sample may be metallized. Therefore, we believe that the subtle variation of the crystal structure is consistent with the transformed dielectric properties. As displayed in Fig. 2b, the conductivity variation with increasing pressure can be separated into three distinct regions: (i) a completely semiconductor (SC) area up to ~6 GPa, (ii) an intermediate state (IS) of a semiconductor and metal between ~6 and ~11 GPa, and (iii) a metal zone above ~11 GPa, which is similar to previous results.[35] The presence of the intermediate region may be due to phonon softening.[36] The pressure-induced interaction between electrons and phonons, which causes electron transfer between layers and deforms the structure, can destroy the symmetry of the crystal. In fact, some semiconductor materials also exhibit an IS in the process of metallization[15] or under pressure[37] because of phonon softening. Interestingly, the conductivity of α-As_2Te_3 after decompression remained higher than 1 S cm^{-1} (Fig. 2b). These conductivity results provide a clue that this transformation was irreversible before and after compression, which is also consistent with our previously reported results on molybdenum disulfide with a similar layered structure.[15] Furthermore, the temperature-dependent conductivity measurements were also performed in a DAC to mutually verify these results.

As shown in Fig. 3a, under pressure of 0–11 GPa, the conductivity of α-As_2Te_3 increases with an increasing temperature under non-hydrostatic conditions, which is a typical characterization of a semiconductor. In contrast, after the phase transition, the conductivity decreases with an increasing temperature above 11 GPa, displaying typical behaviour of a metal (Fig. 3b). Furthermore, we found that the metallicity retains after decompression (Fig. 3d). However, after metallization (Fig. 3c) and decompression under hydrostatic conditions, the conductivity of the sample increases with an increasing temperature, proving that the metallization is reversible under hydrostatic conditions (Fig. 3e). Therefore, metallization in α-As_2Te_3 was observed at a high pressure, which was clearly reversible and irreversible under hydrostatic and non-hydrostatic conditions, respectively.

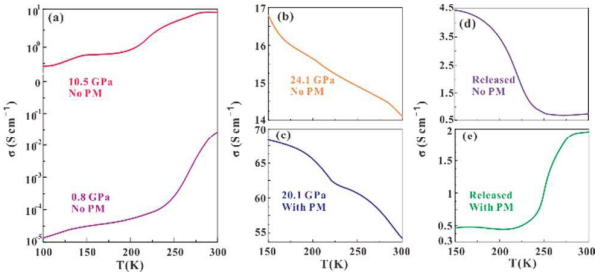

Fig. 3 The temperature-dependent measurements of α-As_2Te_3. (a) α-As_2Te_3 in the semiconducting state under non-hydrostatic conditions. (b) The metallic state of α-As_2Te_3 under non-hydrostatic conditions. (c) The metallization of α-As_2Te_3 under hydrostatic conditions. (d) The metallic state of α-As_2Te_3 after decompression under non-hydrostatic conditions. (e) The semiconducting state of α-As_2Te_3 after decompression under hydrostatic conditions.

Meanwhile, this metallization is consistent with the amorphization of the sample at this pressure point. In fact, previous studies have shown that amorphous states exhibit better conductivities than crystalline phases.[38-39] Due to the open structure of glasses, the conductivity of the amorphous state is generally higher than that of the crystal phase. The electron and ion mobilities will be enhanced when the long-range order of the lattice changes to long-range correlated disorder, as the transformation

View Article Online
DOI: 10.1039/C7TC03309E

will introduce local impurity energy levels into the forbidden band. Thus, the electrical conductivity of the sample will increase after amorphization. On the other hand, as indicated by Zhuang *et al*., the variation of the pressure environment plays a crucial effect on the electrical properties of metallic sulphides with layered structures.[15] In the present study, a hydrostatic methanol and ethanol mixture was used as a pressure medium to alleviate the interlayer interactions due to the entry of this medium into the interlayer space at high pressure. In addition, the layer distance will recover with the pressure medium molecules escape after decompression.[40] In contrast, a stronger interaction will be

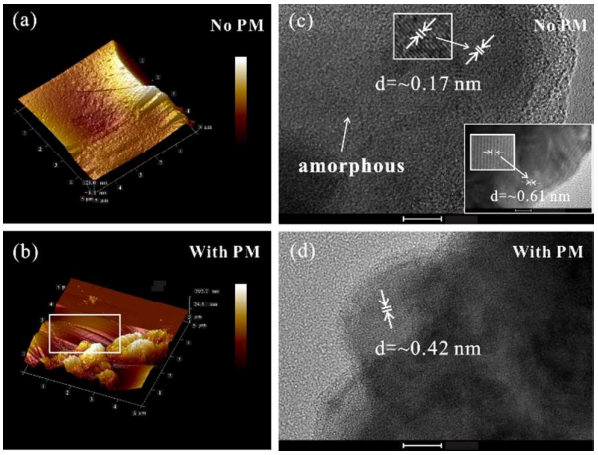

Fig. 4 (a), (b) AFM images of the pressure-induced morphologies of decompressed α-As_2Te_3 from 24.8 GPa under non-hydrostatic conditions and 24.5 GPa under hydrostatic conditions, respectively. (c), (d) HRTEM images of decompressed α-As_2Te_3 from 25.1 GPa under non-hydrostatic conditions and 24.9 GPa under hydrostatic conditions, respectively. Inset: HRTEM image of the initial sample. Scale bar, 10 nm.

generated in the interlayer of α-As_2Te_3 without the protection of pressure medium molecules under non-hydrostatic conditions, which may result in an irreversible reduction of the interlayer spacing.[41-42]

To reveal the morphology and structural change of α-As_2Te_3 after amorphization and metallization, AFM and HRTEM were applied to the recovered samples (Fig. 4). From Fig. 4a, the surface-layered morphology of α-As_2Te_3 was destroyed after decompression from 24.8 GPa under non-hydrostatic conditions. However, as for hydrostatic conditions from 24.5 GPa, the surface-layered morphology of the sample was well preserved and could be clearly discriminated after decompression (Fig. 4b). According to the AFM images of hydrostatic conditions, we can roughly estimate, via the height and the number of layers, an interlayer spacing of ~0.41 nm. In addition, the HRTEM analysis indicated that the original interlayer spacing of α-As_2Te_3 was ~0.61 nm (Fig. 4c, inset). After decompression from 25.1 GPa, most of the sample transformed to an amorphous state with an ~0.17 nm interlayer spacing in the residual layered structure under non-hydrostatic conditions (Fig. 4c). However, the layered structure of α-As_2Te_3 was perfectly preserved upon decompression from 24.9 GPa under hydrostatic conditions (Fig. 4d). At the same time, to disclose the existence of phase state for the recovered sample, a series of representative cross-sectional selected-area electron diffraction patterns by HRTEM were also conducted for starting material and its corresponding high-pressure phases (Fig. 5). As displayed by Fig. 5a and 5b, the irreversible amorphous phase of As_2Te_3 after

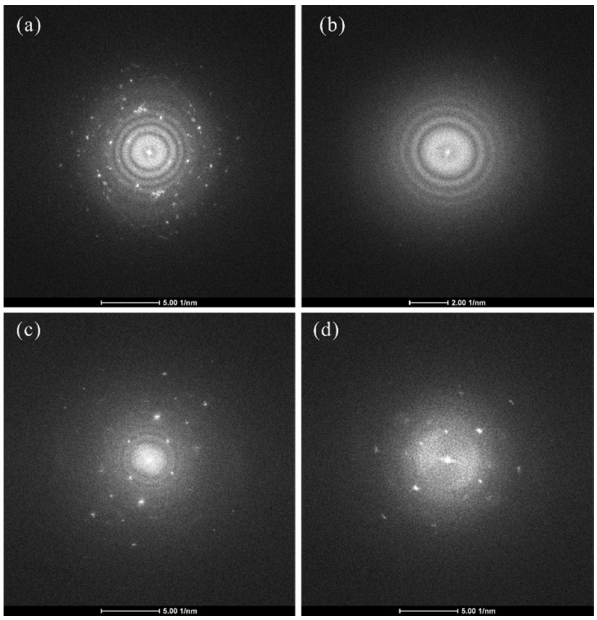

Fig. 5 Representative cross-sectional selected-area electron diffraction patterns by HRTEM for starting As_2Te_3 and its corresponding high-pressure phases. (a) Starting material. (b) The irreversible amorphous phase of As_2Te_3 after decompression from 24.8 GPa under non-hydrostatic pressure. (c) The reversible recovered crystalline phase after decompression from 12.5 GPa under non-hydrostatic pressure (d) The reversible recovered crystalline phase after decompression from 24.5 GPa under hydrostatic pressure.

decompression from 24.8 GPa was confirmed again under non-hydrostatic pressure. However, for two recovered crystalline phases after decompression from 12.5 GPa under non-hydrostatic pressure and from 24.5 GPa under hydrostatic pressure, both of them are reversible (Fig. 5c and 5d).

In addition, the interlayer spacing by HRTEM was ~0.42 nm, which is in good agreement with the AFM results. These results clearly demonstrate that the crystalline-to-amorphous transformation and the reduced interlayer spacing were irreversible under non-hydrostatic conditions. Furthermore, the metallization of α-As_2Te_3 was induced by the overlap of the conduction band and valence band, which resulted from the decreased interlayer spacing.[43-44] Therefore, the AFM and HRTEM images provide good evidence that these irreversible phenomena were owing to the effect of the pressure medium. The molecular diameters of methanol and ethanol in the pressure medium are ~0.27 nm and ~0.34 nm, respectively.[45] Therefore, the pressure medium can enter the interlayer space to weaken the interlayer interactions, protect the layered structure of α-As_2Te_3 and allow the changed interlayer spacing to be reversible under hydrostatic conditions. However, we

View Article Online
DOI: 10.1039/C7TC03309E

also confirmed that α-As_2Te_3 endured an irreversible PIA and metallization under non-hydrostatic conditions.

Conclusions

We systematically investigated the structural, vibrational and electronic properties of α-As_2Te_3 at high pressure and room temperature using a series of experiments, including impedance spectroscopy, temperature-dependent conductivity measurements, high-pressure Raman spectroscopy, AFM and HRTEM. In this study, α-As_2Te_3 transformed into the β-As_2Te_3 structural phase at approximately 6 GPa under non-hydrostatic conditions. In addition, a crystalline-to-amorphous transformation occurred at approximately 11 GPa, accompanied by a transition from a semiconductor to a metal. Interestingly, the amorphization and metallization of α-As_2Te_3 were irreversible under non-hydrostatic conditions. However, under hydrostatic conditions, the structural phase transition of α-As_2Te_3 was delayed by approximately 2 GPa, and the amorphization and metallization were reversible. In this regard, we emphasize that the pressure medium serves as the critical factor to reduce the deviatoric stresses and mitigate the interlayer interactions. These high-pressure behaviours displayed for α-As_2Te_3 will help us understand universal crystal structure evolution and electrical property patterns for these A_2B_3-type compounds, which may have potential applications in opto-electronics devices.

Acknowledgements

This research was financially supported by the Strategic Priority Research Program (B) of the Chinese Academy of Sciences (XDB 18010401), Key Research Program of Frontier Sciences of the Chinese Academy of Sciences (QYZDB-SSW-DQC009), “135” Program of the Institute of Geochemistry of CAS, Hundred Talents Program of CAS and NSF of China (41474078, 41774099 and 41772042).

References

1 O. Mishima, L. D. Calvert and E. Whalley, *Nature*, 1984, **310**, 393–395.
2 S. K. Deb, M. Wilding, M. Somayazulu and P. F. McMillan, *Nature*, 2001, **414**, 528–530.
3 D. Machon, F. Meersman, M. C. Wilding, M. Wilson and P. F. McMillan, *Prog. Mater. Sci.*, 2014, **61**, 216–282.
4 R. J. Hemley, L. C. Chen and H. K. Mao, *Nature*, 1989, **338**, 638–640.
5 R. J. Hemley, A. P. Jephcoat, H. K. Mao, L. C. Ming and M. H. Manghnani, *Nature*, **334**, 1988, 52 – 54.
6 L. Wu, L. Dai, H. Li, H. Hu, Y. Zhuang and K. Liu, *J. Appl. Phys.*, 2017, **121**, 125901.
7 L. E. McNeil and M. Grimsditch, *Phys. Rev. Lett.*, 1992, **68**, 83–85.
8 C. A. Perottoni and J. A. H. da Jornada, *Science*, 1998, **280**, 886–889.
9 T.J. Scheidemantel, J. F. Meng and J.V. Badding, *J. Phys. Chem. Solids*, 2005, **66**, 1744–1747.
10 H. Deng, *J. Alloy. Compd.*, 2016, **656**, 695–701.
11 G. J. Carron, *Acta Cryst.*, 1963, **16**, 338–343.
12 Y. Sharma and P. Srivastava, *Opt. Mater.*, 2011, **33**, 899–904.
13 Z. Zhao, H. Zhang, H. Yuan, S. Wang, Y. Lin, Q. Zeng, G. Xu, Z. Liu, G. K. Solanki, K. D. Patel, Y. Cui, H. Y. Hwang and W. L. Mao, *Nat. Commun.*, 2015, **6**, 7312.
14 S. Duwal and C.-S. Yoo, *J. Phys. Chem. C*, 2016, **120**, 5101–5107.
15 Y. Zhuang, L. Dai, L. Wu, H. Li, H. Hu, K. Liu, L. Yang and C. Pu, *Appl. Phys. Lett.*, 2017, **110**, 122103.
16 M. B. Kruger, Q. Williams and R. Jeanloz, *J. Chem. Phys.*, 1989, **91**, 5910–5915.
17 H. Sankaran, S. K. Sikka, S. M. Sharma and R. Chidambaram, *Phys. Rev. B*, 1988, **38**, 170–173.
18 Y. Fujii, M. Kowaka and A. Onodera, *J. Phys. C: Solid State Phys.*, 1985, **18**, 789–797.
19 J. S. Tse, D. D. Klug, J. A. Rlpmeester, S. Desgreniers and K. Lagarec, *Nature*, 1994, **369**, 724–727.
20 J. S. Tse and D. D. Klug, *Science*, 1992, **255**, 1559–1561.
21 A. Jayaraman, *Rev. Mod. Phys.*, 1983, **55**, 65–108.
22 L. Dai, H. Hu, H. Li, J. Jiang and K. Hui, *Am. Mineral.*, 2014, **99**, 1420–1428.
23 H. Hu, L. Dai, H. Li, K. Hui and J. Li, *Solid State Ionics*, 2015, **276**, 136–141.
24 M. Li, C. Gao, G. Peng, C. He, A. Hao, X. Huang, D. Zhang, C. Yu, Y. Ma and G. Zou, *Rev. Sci. Instrum.*, 2007, **78**, 075106.
25 V. P. Cuenca-Gotor, J. A. Sans, J. Ibáñez, C. Popescu, O. Gomis, R. Vilaplana, F. J. Manjón, A. Leonardo, E. Sagasta, A. Suárez-Alcubilla, I. G. Gurtubay, M. Mollar and A. Bergara, *J. Phys. Chem. C*, 2016, **120**, 19340–19352.
26 N. Sakai and H. Fritzsche, *Phys. Rev. B*, 1977, **15**, 973–978.
27 A. Bera, K. Pal, D. V. S. Muthu, S. Sen, P. Guptasarma, U. V. Waghmare and A. K. Sood, *Phys. Rev. Lett.*, 2013, **110**, 107401.
28 R. Vilaplana, D. Santamaría-Pérez, O. Gomis, F. J. Manjón, J. González, A. Segura, A. Muñoz, P. Rodríguez-Hernández, E. Pérez-González, V. Marín-Borrás, V. Muñoz-Sanjose, C. Drasar and V. Kucek, *Phys. Rev. B*, 2011, **84**, 184110.
29 J. S. Tse, D. D. Klug, C. A. Tulk, I. Swainson, E. C. Svensson, C.-K. Loong, V. Shpakov, V. R. Belosludov, R. V. Belosludov and Y. Kawazoe, *Nature*, 1999, **400**, 647–649.
30 M. B. Kruger and R. Jeanloz, *Science*, 1990, **249**, 647.
31 Q. Williams and R. Jeanloz, *Nature*, 1989, **338**, 413–415.
32 S. Klotz, J. C. Chervin, P. Munsch and G. Le Marchand, *J. Phys. D: Appl. Phys.*, 2009, **42**, 075413.
33 X. Q. Yan, Z. Tang, L. Zhang, J. J. Guo, C. Q. Jin, Y. Zhang, T. Goto, J. W. McCauley and M. W. Chen, *Phys. Rev. Lett.*, 2009, **102**, 075505.
34 Y. A. Kandrina, A. N. Babushkin, S. N. Shkerin and Y. Volkova, *Defect Diffus. Forum*, 2002, **208–209**, 295–298.
35 J. Zhao, L. Yang, Z. Yu, Y. Wang, C. Li, K. Yang, Z. Liu and Y. Wang, *Inorg. Chem.*, 2016, **55**, 3907–3914.
36 H. J. Conley, B. Wang, J. I. Ziegler, R. F., Jr. Haglund, S. T. Pantelides and K. I. Bolotin, *Nano. Lett.*, 2013, **13**, 3626–3630.
37 J. Yan, E. A. Henriksen, P. Kim and A. Pinczuk, *Phys. Rev. Lett.*, 2008, **101**, 136804.
38 D. Umeyama, S. Horike, C. Tassel, H. Kageyama, Y. Higo, K. Hagi, N. Ogiwara and S. Kitagawa, *APL Mater.*, 2014, **2**, 124401.
39 M. Tatsumisago and A. Hayashi, *Solid State Ionics*, 2012, **225**, 342–345.
40 S. Jiménez Sandoval, D. Yang, R. F. Frindt and J. C. Irwin, *Phys. Rev. B*, 1991, **44**, 3955–3962.
41 P. E. Kalita, S. V. Sinogeikin, K. Lipinska-Kalita, T. Hartmann, X. Ke, C. Chen and A. Cornelius, *J. Appl. Phys.*, 2010, **108**, 043511.

View Article Online
DOI: 10.1039/C7TC03309E

42 R. P. Dias, M. Kim and C.-S. Yoo, *Phys. Rev. B*, 2016, **93**, 104107.
43 X. Zhang, X. F. Qiao, W. Shi, J. B. Wu, D. S. Jiang and P. H. Tan, *Chem. Soc. Rev.*, 2015, **44**, 2757–2785.
44 W. Ju, T. Li, H. Wang, Y. Yong and J. Sun, *Chem. Phys. Lett.*, 2015, **622**, 109–114.
45 S. Darvishmanesh, A. Buekenhoudt, J. Degrève and B. Van der Bruggen, *Sep. Purif. Technol.*, 2009, **70**, 46–52.

View Article Online
DOI: 10.1039/C7TC03309E

Graphical abstracts (table of contents entry)

A crystalline to amorphous and metallic transition was demonstrated by impedance spectroscopy, Raman spectroscopy, AFM and HRTEM in DAC.